International Journal of Heat and Mass Transfer 71 (2014) 189–196

Contents lists available at ScienceDirect

International Journal of Heat and Mass Transfer

journal homepage: www.elsevier.com/locate/ijhmt

An experimental investigation of enhanced pool boiling heat transfer from surfaces with micro/nano-structures

Lining Dong, Xiaojun Quan, Ping Cheng *

MOE Key Laboratory for Power Machinery and Engineering, School of Mechanical Engineering, Shanghai Jiao Tong University, Shanghai 200240, PR China

ARTICLE INFO

Article history:
Received 4 November 2013
Received in revised form 22 November 2013
Accepted 22 November 2013
Available online 4 January 2014

Keywords:
Pool boiling
Micro/nano-structures
Nucleation site
Bubble departure
Heat transfer coefficient

ABSTRACT

Experiments on subcooled and saturated pool boiling of ethanol are conducted on horizontal heated surfaces with micro- and nano-sized structures. The effects of structure size on bubble nucleation and departure characteristics as well as the heat transfer coefficient are discussed. It is found that microstructures can enhance bubble nucleation by significantly increasing the active nucleation site density at low heat fluxes, thus reducing the wall superheat and enhancing heat flux; while nano-structures can accelerate bubble departure by decreasing bubble departure diameter and increasing departure frequency. On the other hand, nano-structures will delay bubble mergence and prevent the vapor film from spreading at high heat fluxes during boiling crisis.

1. Introduction

With advances in micro-fabrication and surface treatment technology, microstructures (such as micro-pillars and micro cavities) and nanostructures (such as nanoporous coating, carbon nanotubes, Cu/CuO nanowires, silicon nanowires) have recently been fabricated on heated surfaces for the possibility of enhancing nucleate boiling heat transfer [1,2]. Experimental results [3–12] did show that surfaces with micro and nano-structures enhance the heat transfer coefficient and critical heat flux (CHF), compared with bare surfaces. The following is a summary of literature on various effects of micro- and nano-surface structures on nucleate boiling heat transfer:

1.1. The increase in heat transfer area

It is obvious that micro and nano-structures with large surface-area-to-volume ratio can enlarge the effective area for heat transfer. In order to study the effect of the increase in heat transfer area on boiling enhancement, Guglielmini et al. [10] as well as Yu et al. [11,12] defined heat flux and heat transfer coefficient based on the real area of rough surfaces as q_r and h_r. Their experiments of FC-72 saturated boiling from micro-pillars and micro-cavities found that the effect of microstructures on q_r and h_r were not apparent at low heat flux, while the microstructures can obviously enhance heat transfer coefficient and CHF at high heat flux. They concluded that the increase of heat transfer area of the microstructures was the main reason for boiling enhancement at low heat fluxes, but they could not explain the significant improvement of heat transfer coefficients at high heat fluxes. It appears, therefore, there are different mechanisms for enhanced nucleate boiling heat transfer in the low heat flux and high heat flux regimes.

1.2. The increase in active nucleation site density

Previous experimental studies [13–15] showed that the active nucleation site density was determined by the surface micro-roughness, wettability, heat flux or wall superheat. Garimella and co-workers [16,17] found that surface micro and nanostructures could increase the number of active nucleation sites in pool boiling. Yang and Kim [18] developed an integral expression for nucleation site density as a product of cavity mouth radius and cavity angle. Wang and Dhir [13] found that the active nucleation site density was increased with the smaller-sized cavities on the surface, and proposed an empirical correlation of nucleation site density in terms of the micro-cavity radius and contact angle. However, it was uncertain whether this correlation of nucleation site density was applicable for nanostructure surface.

1.3. The increase in bubble departure frequency

Micro and nano-sized structures also influence the bubble nucleation and bubble departure. Li et al. [19] as well as Chen et al. [20] observed nucleate boiling phenomena on surfaces with Cu and TiO_2 nanotubes, respectively. Compared with smooth surfaces, they

* Corresponding author. Tel./fax: +86 21 34206337.
E-mail addresses: pingcheng@sjtu.edu.cn, ijhmt.cn@sjtu.edu.cn (P. Cheng).

0017-9310/$ - see front matter © 2013 Elsevier Ltd. All rights reserved.
http://dx.doi.org/10.1016/j.ijheatmasstransfer.2013.11.068

found that density of active nucleation sites was considerably increased on nano-structured surfaces at the same wall superheat. They also found that the bubble departure diameter decreased and departure frequency increased on surfaces with nanotubes at low-heat-flux region. However, these conclusions were contradictory with those given by McHale and Garimella [16], who found that the bubble departure frequencies change only slightly on micro-structured surfaces compared with smooth surfaces.

From the above summary of literatures, it is known that micro/nano-sized structures will increase the heat transfer area, and influence bubble nucleation on and bubble departure from the surface. But the mechanisms for changes in nucleation sites and departure frequency for enhanced nucleate boiling heat transfer has not been clarified. From our previous thermodynamic analysis on heterogeneous nucleation [21], it was demonstrated that bubble nucleation on a roughness surface depended not only on wall superheat (or heat flux) but also the curvature radius of microstructures as well. Thus, effects of structure size and amount of heat flux must be taken into consideration simultaneously when analyzing the mechanism for boiling enhancement on structured surfaces.

In this paper, the bubble dynamic behaviors during nucleation on and departure from micro/nano-structured surfaces are observed using a high-speed visualization system. Effects of these structures on nucleation sites density and departure frequency are presented to clarify the mechanisms for enhancing nucleate boiling heat transfer at low and high heat flux regimes, respectively.

2. Experimental setup

2.1. Experimental system

Fig. 1 shows that the experimental system consisted a test section (a silicon chip) in a large chamber, a temperature control system, a visualization system, and a data acquisition system. Ethanol was used as the working fluid. The walls of the chamber were made of optical glasses (with thickness of 10 mm) to facilitate visualization. The volume of the chamber was $150 \times 150 \times 150\ mm^3$, which was sufficiently large in comparison with the chip which was 15×15 mm ($A_{pool}/A_{chip} = 100$). At the bottom of the chamber, a water bath was used to control the liquid subcooling temperature, while another water bath with coolant was used at the top of chamber to condense the vapor of ethanol. The chip was heated by integrated Pt resistors at its bottom. A PTFE column with 45×45 mm in diameter and height was attached to the chip to prevent heat loss.

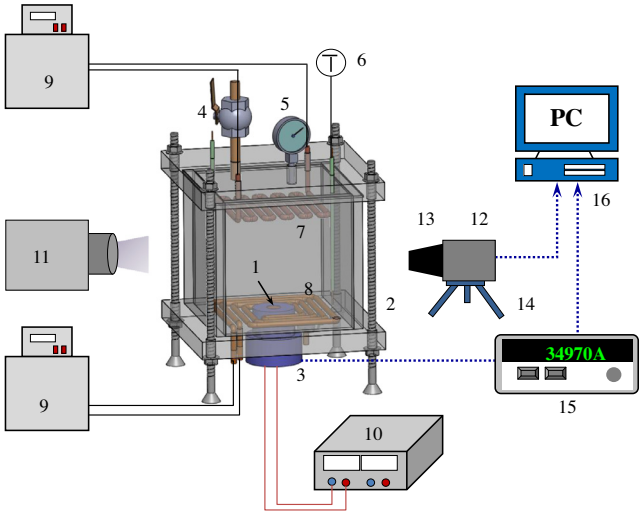

1. Test chip	2. Glass chamber	3. PTFE block	4. Valve
5. Pressure gage	6. Thermocouple	7. Condenser pipe	8. Copper pipe
9. Water baths	10. AC power	11. Illuminator	12. CCD
13. Microscope	14. Tripod and holder	15. Data acquisition system	16. Computer

Fig. 1. Experimental setup of pool boiling.

The visualization system contained a high-speed CCD camera (X-stream™ XS-4), microscope lens, a Nikon fiber illuminator, and some other accessories. In order to take photos from both the lateral and top positions, tripod and holder were used to support the camera and control the location of the microscope. The chamber was filled with ethanol and the pressure in the chamber was measured with a pressure gage and maintained at the atmospheric pressure through the valve. The ethanol temperature in the chamber was measured by a T-type thermocouple. The wall temperature of Si chip was measured with Pt sensors integrated at the bottom of test section. All of the temperature and voltage signals were collected by an Agilent data acquisition system.

2.2. Test section

MEMS technology was used to fabricate the test section on a ⟨100⟩ silicon wafer of 0.5 mm in thickness. The average roughness of bare chip was about $R_a = 0.217$ nm, which was considered to be a smooth surface in this paper. As shown in Fig. 2(a)–(d), four types of structures were fabricated on test chips: micro-pillars (MP), micro-cavities (MC), nanowires (NW) and nano-cavities (NC).

Silicon chips with micro-pillars and micro-cavities were prepared through a dry etching process while nanowires and nano-cavities were fabricated with the aid of etching solutions containing $AgNO^3$ and hydrofluoric acid [22,23]. The concentration of Ag^+ in the aqueous solution determined the porosity of nano-structures. The heights of both micro- and nano-sized structures (H) were controlled by the etching time. The geometry parameters and values of contact angle for test chips are listed in Table 1. At the bottom of the silicon chip, a thin film of TiW was sputtered, followed by Pt film of 200 nm and Au leader of 300 nm in thickness, respectively. Integrated Pt resistors were used as heaters and temperature sensors simultaneously.

2.3. Data reduction

The temperature of present experiments was in the range of 20–200 °C. The wall temperature T_w could be determined according to the relationship between the Pt resistance and temperature. The linear correlation of R_{Pt} and T_{Pt} ($R_{Pt} = aT_{Pt} + b$) was determined by placing a standard thermocouple and the Pt resistance in a constant temperature oven. T_{Pt} was measured by the standard thermocouple, and R_{Pt} is given by

$$R_{Pt} = U_{Pt}/I \tag{1}$$

where I and U_{Pt} are the electric current and voltage of Pt heater, respectively. A reference resistor with standard values ($R_{ref} = 1\Omega$, 10Ω) was used to measure the electric current, which is given as

$$I = U_{ref}/R_{ref} \tag{2}$$

The voltages of Pt resistors and the reference resistor were measured and collected by an Agilent data acquisition system.

The heat flux of the integrated Pt heater is calculated by the heating power per unit area, i.e.,

$$q = Q/A \tag{3a}$$

where the heating power of Pt heater is given by $Q = U_{Pt}I$. With the aid of Eq. (2), the heat flux can be calculated as

$$q = \frac{U_{Pt}U_{ref}}{AR_{ref}} \tag{3b}$$